Published in "Journal of Archaeological Science 33(3): 440-452, 2006"
which should be cited to refer to this work.

The glass-melting crucibles of Derrière Sairoche (1699−1714 AD, Ct. Bern, Switzerland): a petrological approach

Giacomo Eramo*

Département de Géosciences, Minéralogie et Pétrographie, Université de Fribourg, Chemin du Musée 6, CH-1700 Fribourg, Switzerland

Received 23 August 2004; received in revised form 28 June 2005; accepted 6 September 2005

Abstract

Forty-three sherds of crucible found in the pre-industrial (1699−1714 AD) forest glassworks of Derrière Sairoche (Ct. Bern, Switzerland) were studied in order to determine the nature of raw materials and the technological aspects of their production and use. The samples were analysed using optical microscopy, XRD, XRF, UV−VIS spectrometry and SEM/EDS.

The crucibles were produced with local natural clayey sand and fired in two steps. After preliminary firing in a low-temperature furnace (800−1000 °C), the crucibles were brought to temperatures up to 1500 °C within the glass-melting furnace, before adding the glass batch. Using the structural order of cristobalite as an archaeothermometer, temperatures between 1370 and 1500 °C were estimated. The crucible surface shows corrosion by glass and furnace gases. Connections between glassmaking and crucible production are emphasised by this study.

Keywords: Glass-melting crucibles; Cristobalite; Swiss Jura; Pre-industrial glassworks

1. Introduction

Crucibles are as important as melting furnaces in glassmaking. Good crucibles provide refractory behavior (high softening point), no chemical contamination (very low concentration of transition metals) and mechanical strength (thermal shock resistance). Since the Middle Ages, many treatises on glass discussed crucibles as fundamental tools in getting good quality glass. Theophilus (12th century) suggested making crucibles with a ''white clay'' and once dry, putting them in the ''incandescent furnace'' [23].

In *De la pirotechnia* (1540) Biringuccio [41] wrote that both the crucibles and the refractory lining of the melting furnace were made from the same fire-resistant clay (i.e. Valencia clay and Treguanda clay). After a long drying period (six or eight months), crucibles were heated in the fritting oven until they became red-hot, and then were moved with tongs, as quickly as possible, to the melting furnace for the last heating. Merret [30] in his translation of *L'Arte vetraria* by A. Neri (1612), quotes some source of refractory clays in England and describes the way they should be processed to get good crucibles. A distinction between large pots for *cristallo* and small pots for colored glass was made as well. The *Encyclopédie* by Diderot and D'Alembert [11] dedicated volume 17 to glassmaking. In addition to a description of the operating chain in glass production, they also showed how to build the furnaces and make pots. The recycling of broken crucibles as temper for new crucibles and for refractory materials was suggested to reduce shrinkage. Crucibles were fired in two steps in a similar way as reported by Biringuccio [41].

These authors recommended maximum care for crucible production and for the construction of the melting furnace. The technology for producing crucibles depends on glass composition. During the Roman period, the glass had lower liquidus temperatures (900−1100 °C) and common ware could be used as crucibles [24,36,40], while in the Middle Ages, crucibles were produced starting from silicatic raw materials able to yield during firing a phase association stable at high temperatures. The technological and pyrotechnological evolution caused by the higher liquidus temperatures (1000−1400 °C) of wood-ash glass demanded more performing raw

* Tel.: +41 26 300 89 44; fax: +41 26 300 97 65.
E-mail address: giacomo.eramo@unifr.ch

materials and a better exploitation of combustibles [6,7,13,45]. Owing to this technological dependence glass, crucibles and melting furnace can be considered as parts of the same system, as well as the pyrotechnology needed to melt a given glass. For these reasons in northern European glasshouses, each part was managed by glassmakers [7,31,34].

2. Crucibles from Derrière Sairoche

In the Jura region, dozens of pre-industrial glassworks (17th−19th century) have been localised by historical and archaeological researches [2,17−19]. Excavations carried out by the Archaeological Survey of the Canton Bern in the glassworks of Derrière Sairoche (1699−1714 AD), one of four glassworks situated in the Chaluet Valley (Court) (Fig. 1), brought to light the workshop area and the glassmakers' dwellings [17−19]. Between 2000 and 2003, in the workshop area, a great quantity of small fragments of crucibles was found. In five cases it was possible to restore the crucibles and get an idea of the original features (Fig. 2). Although the restored crucibles are typologically the same, some differences in shape and dimension, exclude forming in mould. Hence, the crucibles were formed almost certainly by coil-building technique, as is still used in modern times for artistic glassmaking [20]. The operative volume, calculated on the base of their mean dimensions (Fig. 3), is about 15 l. The oval shape was useful to save space in the melting chamber and to place the crucibles into the furnace through narrow apertures. The melting furnace of Derrière Sairoche had 10 glory holes in the sidewalls, which corresponded to five crucibles per siege [2] (Fig. 4). The use at high temperatures left different wear marks on the crucibles. The corrosive effect of glass on the crucible body is more evident on the inner surface, which was continuously in contact with it, whereas the outer surface reveals shrinkage crack networks (Fig. 5) according to the closeness to the flame and shows surface vitrification. The wall thickness is

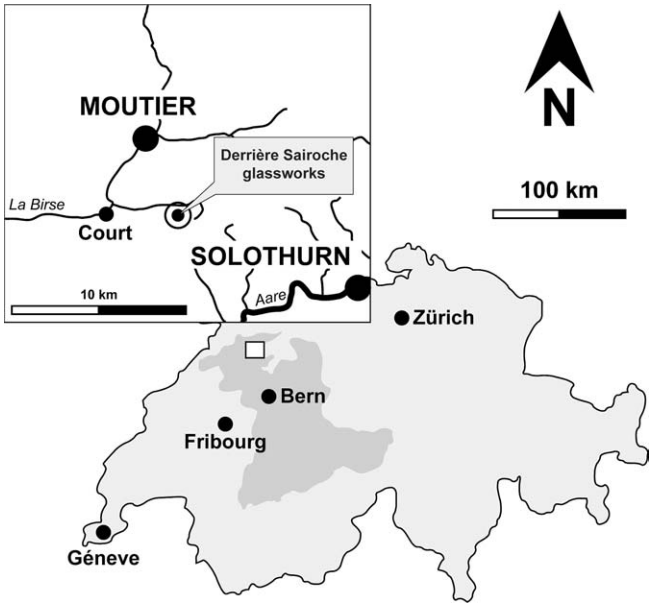

Fig. 1. The glassworks of Derrière Sairoche in Canton Bern (shaded area).

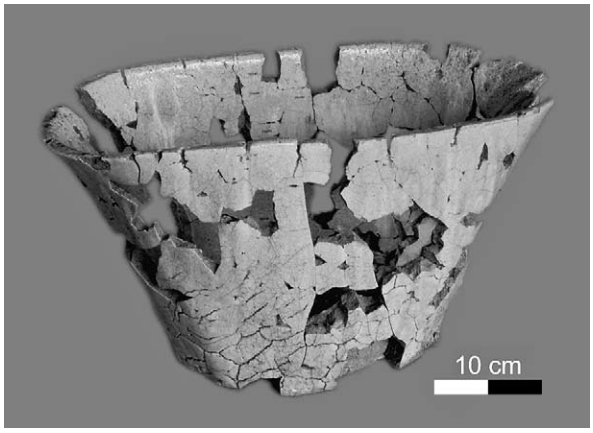

Fig. 2. A restored glass-melting crucible from Derrière Sairoche.

about 3 cm next to the bottom decreasing to as little as 1 cm in the rim. The opposite curved parts of the wall (long axis) are yellow-orange and grey, respectively. In each crucible the grey core corresponds to the surface parts with more fracture network. These observations were helpful in figuring out the position of the 43 analysed fragments within the pot and lead to a better understanding of the technological aspects concerning both crucible production and use. The crucible body is not homogeneous. Generally, one can distinguish the crystalline core, the inner surface in contact with batch glass and the outer vitrified surface (Fig. 6). By analysing the core, it is possible to answer the questions concerning the nature of the raw materials, the way they were processed and the transformations that occurred during firing and use. The surfaces, on the other hand, provide some information about the interaction with the exterior in the melting furnace. A petrological approach to the study was useful to (1) determine the original mineral composition of the crucibles; (2) demonstrate whether or not broken crucibles were used as temper; (3) estimate the temperature range to which the crucibles were exposed; (4) prove whether crucibles were fired and used in the melting furnace; (5) investigate the effect of chemical contamination on the surface of the crucible body.

A description of the analytical methods is provided in Appendix 1.

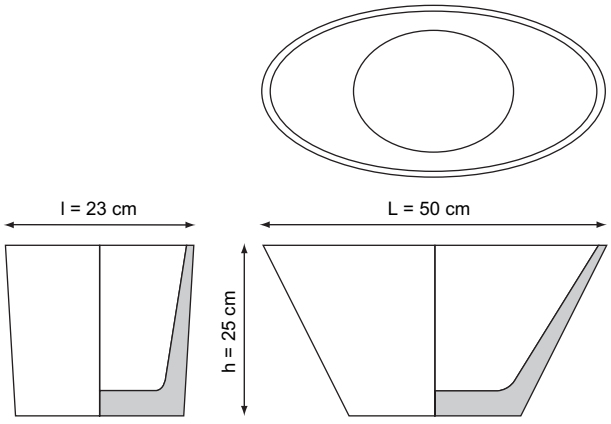

Fig. 3. Graphical reconstruction based on the mean dimensions of the restored crucibles.

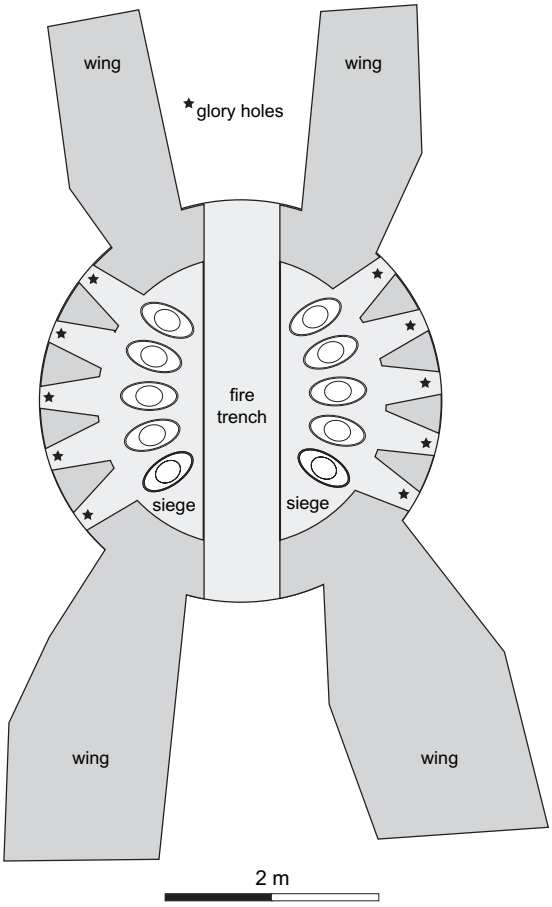

Fig. 4. Schematic plan of the melting furnace of Derrière Sairoche, showing the position of the crucibles during its activity.

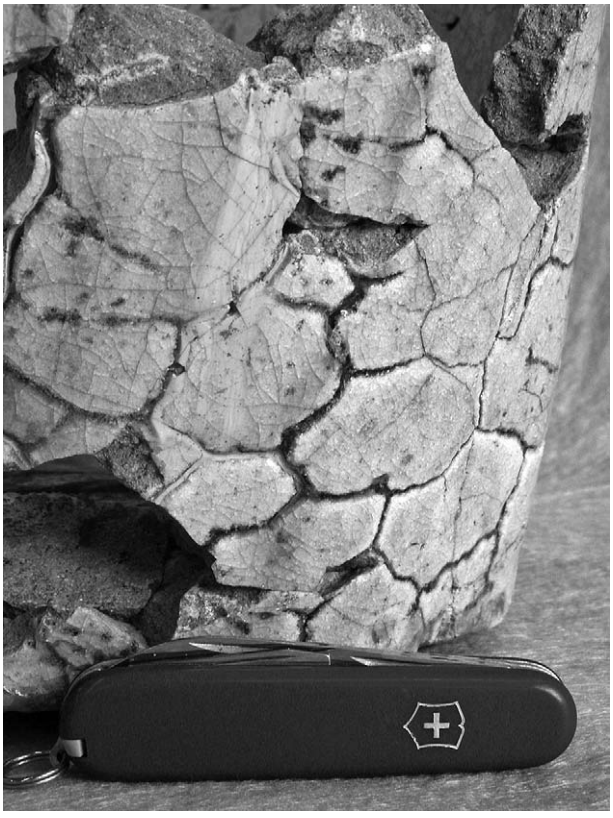

Fig. 5. Side of the crucible close to flame. Note the crack network on the surface due to thermal stress.

3. Results

3.1. Original mineral composition

Under the petrographical microscope, monocrystalline quartz is the only recognizable component of the originally non-plastic fraction of the crucibles. Table 1 shows the analysed samples with their relative mineral compositions, obtained by XRD analysis. XRF analyses revealed that SiO_2 and Al_2O_3 occur as major components, followed by TiO_2 which rarely exceeds 1 wt.% (Table 2). The low content of alkali and alkaline earth elements (<1 wt.%) points to an original clay matrix consisting mainly of kaolinite. Thanks to their simple chemical composition, which can be approximated to SiO_2 and Al_2O_3, a theoretical mineralogical composition of the raw materials can be obtained by normative calculation, assigning all Al_2O_3 to kaolinite and the excess of SiO_2 to quartz (Table 3). Normative quartz varies between 76 and 84

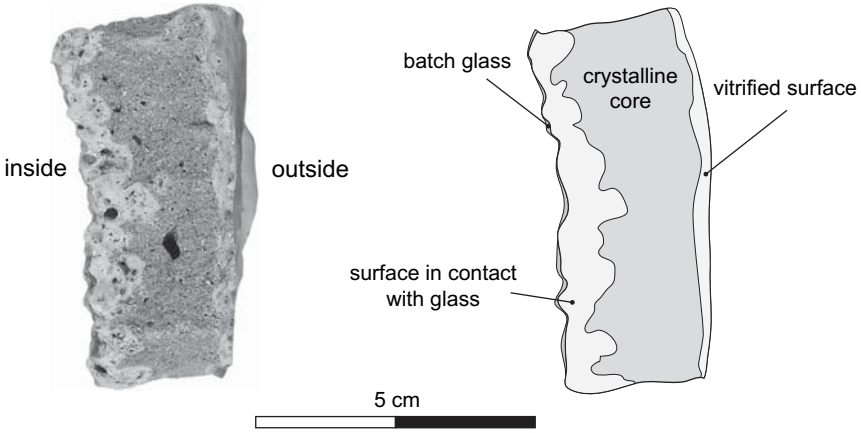

Fig. 6. Photo of sample ER28 (left) and schematic sketch (right) of the three recurrent structural portions: the inner surface in contact with batch glass, the crystalline core and the outer vitrified surface.

Table 1
Macroscopic characteristics and mineral content determined by XRD

Sample	Colour	Thickness (mm)	$d_{(101)}$ Crs (nm)	Mineral content
ER21	grey	27	0.4059	Crs + Qtz + Mul
ER22	yellow	27	0.4061	Crs + Qtz + Trd + Mul
ER23	yellow	25	0.4062	Crs + Qtz + Trd + Mul
ER24	grey	22	0.4062	Crs + Qtz + Trd + Mul
ER25	violet	22	0.4063	Crs + Qtz + Trd + Mul
ER26	yellow	30	0.4062	Crs + Qtz + Trd + Mul
ER27	yellow	25	0.4063	Crs + Qtz + Trd + Mul
ER28	grey	28	0.4059	Crs + Qtz + Trd + Mul
ER29	yellow	36	0.4066	Crs + Qtz + Mul
ER30	yellow	31	0.4063	Crs + Qtz + Trd + Mul
ER31	grey	25	0.4059	Crs + Qtz + Trd + Mul
ER32	grey	35	0.4064	Crs + Qtz + Trd + Mul
ER33	yellow	27	0.4060	Crs + Qtz + Trd + Mul
ER34	yellow	32	0.4061	Crs + Qtz + Trd + Mul
ER35	yellow	16	0.4064	Crs + Qtz + Trd + Mul
ER36	grey	27	0.4064	Crs + Qtz + Trd + Mul
ER37	grey	18	0.4060	Crs + Qtz + Trd + Mul
ER38	yellow	17	0.4064	Crs + Qtz + Trd + Mul
ER39	yellow	31	0.4059	Crs + Qtz + Trd + Mul
ER40	yellow	24	0.4060	Crs + Qtz + Trd + Mul
ER41	grey	24	0.4063	Crs + Qtz + Mul
ER42	grey	18	0.4066	Crs + Qtz + Trd + Mul
ER43	yellow	16	0.4061	Crs + Qtz + Trd + Mul
ER44	yellow	25	0.4064	Crs + Qtz + Trd + Mul
ER45	yellow	23	0.4064	Crs + Qtz + Trd + Mul
ER46	yellow	14	0.4068	Crs + Qtz + Mul
ER47	grey	14	0.4064	Crs + Qtz + Trd + Mul
ER48	grey	13	0.4066	Crs + Qtz + Trd + Mul
ER49	yellow	15	0.4066	Crs + Qtz + Mul
ER50	yellow	16	0.4059	Crs + Qtz + Trd + Mul
ER51	grey	15	0.4066	Crs + Qtz + Trd + Mul
ER52	yellow	11	0.4066	Crs + Qtz + Trd + Mul
ER53	grey	13	0.4066	Crs + Qtz + Trd + Mul
ER54	grey	16	0.4066	Crs + Qtz + Trd + Mul
ER55	grey	15	0.4063	Crs + Qtz + Trd + Mul
ER56	grey	12	0.4066	Crs + Qtz + Trd + Mul
ER57	grey	17	0.4066	Crs + Qtz + Trd + Mul
ER58	yellow	17	0.4064	Crs + Qtz + Trd + Mul
ER59	grey	18	0.4062	Crs + Qtz + Trd + Mul
ER60	yellow	18	0.4061	Crs + Qtz + Trd + Mul
ER61	grey	18	0.4063	Crs + Qtz + Trd + Mul
ER62	yellow	33	0.4059	Crs + Qtz + Trd + Mul
ER65	grey	25	0.4059	Crs + Qtz + Trd + Mul

Mineral abbreviations: cristobalite (Crs); tridymite (Trd); quartz (Qtz); mullite (Mul).

wt.%. As kaolinite and quartz have almost the same density ($\rho_{Qtz} = 2.65$ vs. $\rho_{Kln} = 2.61-2.68$), the normative quantities can be approximated as modal. The grain-size analysis on thin section of the crucibles reported by Eramo [14] shows that the sand fraction ($\varnothing > 63$ μm) is comprised between 31.43 and 75.00 wt.%. Differences between the normative and modal quantities of quartz are due to the fine grains ($\varnothing < 63$ μm) which were not counted in the grain-size analysis in thin section. Furthermore, in the same study, principal component analysis (PCA) applied to grain-size and chemical variables of the crucibles, as well as of the refractory fragments of the melting furnace and of the refractory earth (*Hupper* sand) sampled in proximity of Derrière Sairoche revealed strong affinities between the archaeological samples and some of the raw materials. This means that it was possible to exploit a refractory earth which naturally has the grain-size and chemical features of the crucibles, without any further processing (i.e. tempering or refining).

3.2. Recycling

The crucible fragments found in the workshop area are only few centimetres in size, pointing to an intentional breaking after their use. According to many authors [7,31,34,35], used crucibles were broken, milled and sieved to recycle them as temper. An example of this practice is reported in the plate VII of the *Encyclopédie* by Diderot and D'Alembert [11]. As for the crucibles of Derrière Sairoche, there is no petrographic evidence of crucible fragments in the ceramic body. It must be kept in mind that even if the crucibles were tempered with very fine fragments it is difficult to detect under the microscope, some chemical contamination due to glass adhering to the surface must have been unavoidable. The glass produced in Derrière Sairoche contains about 20 wt.% of CaO and 10 wt.% of K_2O [44,45], while these two oxides do exceed 1 wt.% neither in the crucibles nor in the Hupper sand (Table 2). It should be considered that a hypothetical recycle of 20 wt.% of crucible fragments as temper, contaminated with 10 wt.% of batch glass, would have increased the concentrations of CaO and K_2O, respectively, by 0.50 and 0.25 wt.% in the analysed crucibles. Although this calculation takes into account reasonable quantities of temper and levels of batch glass contamination, CaO and K_2O concentrations in the analysed crucibles do not significantly differ from those of the Hupper sand. The results of PCA reported by Eramo [14], carried out on grain-size and chemical variables, show a good fit between the crucibles and some of the refractory earth and make the recycling of broken crucibles as temper not plausible. On the other hand, breaking up the used crucibles would have been useful to obtain glass fragments to add as cullet to new batches to help the melting process.

3.3. Temperature in service conditions

XRD analysis revealed co-occurrence of α-quartz, α-cristobalite, α-tridymite (absent in ER21, 29, 41, 46 and 49) and orthorhombic mullite (Table 1). The mineralogical reactions responsible for the mineral composition of the crucible fragments are the dehydroxilation reaction of the kaolinite and the polymorphic reactions involving quartz. The phase association obtained by firing kaolinite at $T \geq 1200$ °C is orthorhombic mullite ($Al_6Si_2O_{13}$) and cristobalite [4,5,25,43]. Since cristobalite tends to crystallize or to break up through $\beta \rightarrow \alpha$ inversion into very small crystals [3,41], this feature could explain the amorphous aspect of the matrix of the crucibles observed under the SEM (Fig. 7), although the XRD spectra do not show a high background due to the occurrence of amorphous phase.

As discussed in Eramo [14], the estimation of the maximum temperature reached by the crucible fragments, based

Sample	SiO_2 (wt.%)	TiO_2 (wt.%)	Al_2O_3 (wt.%)	Fe_2O_{3tot} (wt.%)	MnO (wt.%)	MgO (wt.%)	CaO (wt.%)	Na_2O (wt.%)	K_2O (wt.%)	P_2O_5 (wt.%)	Sum (wt.%)	Ba (ppm)	Cl (ppm)	Cu (ppm)	Nb (ppm)	Ni (ppm)	Pb (ppm)	Rb (ppm)	Sr (ppm)	Y (ppm)	Zn (ppm)	Zr (ppm)	LOI (wt.%)
ER21	90.54	0.95	8.39	0.61	<0.01	0.17	0.20	0.80	0.23	0.01	101.98	78	61	3	19	36	14	17	26	14	6	359	0.23
ER22	90.83	0.64	8.27	0.42	<0.01	0.13	0.21	0.51	0.21	0.01	101.28	64	67	16	15	18	<6	10	28	13	3	289	0.10
ER23	87.57	0.97	11.45	0.65	<0.01	0.11	0.22	<0.01	0.26	0.02	101.33	62	91	<2	20	18	<6	11	70	16	4	357	0.13
ER24	90.76	0.64	8.25	0.38	<0.01	0.13	0.22	0.22	0.40	0.01	101.06	73	71	<2	15	32	<6	17	30	12	<2	280	0.11
ER25	90.39	0.76	9.05	0.35	<0.01	0.09	0.19	0.19	0.38	<0.01	101.46	51	62	<2	16	11	<6	14	22	11	<2	252	0.21
ER26	89.34	0.72	9.64	0.38	<0.01	0.09	0.19	<0.01	0.33	0.01	100.76	68	71	<2	14	20	<6	8	19	11	<2	256	0.22
ER27	91.83	0.65	7.65	0.32	<0.01	0.15	0.13	0.18	0.16	<0.01	101.12	65	61	<2	16	17	<6	9	22	12	2	285	0.11
ER28	87.88	0.89	11.11	0.57	<0.01	0.09	0.23	0.15	0.25	0.02	101.23	75	78	<2	19	26	<6	10	24	13	2	278	0.24
ER29	90.21	0.81	9.66	0.51	<0.01	0.09	0.20	0.03	0.07	<0.01	101.65	39	70	<2	15	31	12	5	19	11	5	277	0.15
ER30	91.22	0.63	8.36	0.43	<0.01	0.14	0.23	0.10	0.21	0.01	101.37	50	66	<2	16	20	<6	9	29	14	<2	296	0.11
ER31	90.84	0.64	8.47	0.40	<0.01	0.18	0.18	0.05	0.34	0.01	101.18	78	67	<2	13	37	<6	20	26	12	5	324	0.09
ER32	89.76	0.70	9.40	0.54	<0.01	0.08	0.17	0.06	0.12	0.01	100.88	34	77	4	14	33	<6	4	23	11	<2	294	0.17
ER33	91.38	0.64	8.30	0.42	<0.01	0.13	0.19	0.08	0.20	0.01	101.40	68	75	<2	14	29	8	13	28	14	2	279	0.09
ER34	87.72	0.72	11.45	0.50	<0.01	0.07	0.21	0.09	0.07	<0.01	100.90	65	90	<2	16	24	10	3	29	14	4	292	0.14
ER35	89.84	0.67	9.40	0.32	<0.01	0.11	0.14	0.27	0.28	0.02	101.13	78	68	<2	16	65	<6	17	29	16	<2	289	0.12
ER36	87.22	0.82	11.55	0.34	<0.01	0.07	0.16	0.48	0.54	0.01	101.24	49	84	<2	18	49	<6	21	23	12	<2	305	0.23
ER37	91.50	0.59	7.33	0.33	<0.01	0.15	0.13	0.21	0.26	<0.01	100.58	89	56	<2	15	47	<6	13	21	12	<2	301	0.10
ER38	88.39	0.92	10.20	0.48	<0.01	0.07	0.18	0.05	0.26	0.01	100.62	44	74	<2	17	27	<6	6	18	13	<2	309	0.20
ER39	91.50	0.64	8.55	0.51	<0.01	0.09	0.14	0.46	0.09	<0.01	102.04	45	71	11	14	20	<6	7	21	9	<2	277	0.17
ER40	91.07	0.63	8.31	0.42	<0.01	0.17	0.19	0.17	0.21	0.01	101.26	73	59	<2	15	28	<6	11	27	14	<2	294	0.07
ER41	86.93	0.86	11.58	0.68	<0.01	0.09	0.43	<0.01	0.24	0.01	100.84	70	85	<2	17	27	9	11	28	13	2	286	0.14
ER42	89.92	1.42	8.07	0.57	<0.01	0.23	0.23	0.14	0.27	0.02	100.92	48	67	<2	28	34	9	13	28	15	11	396	0.08
ER43	92.04	0.59	7.35	0.35	<0.01	0.14	0.15	0.20	0.27	0.01	101.16	73	66	<2	15	61	15	16	20	10	<2	299	0.13
ER44	91.19	0.70	8.77	0.35	<0.01	0.12	0.17	0.14	0.16	<0.01	101.67	62	64	<2	17	24	<6	12	21	13	<2	284	0.06
ER45	90.38	0.63	8.52	0.24	<0.01	0.13	0.17	0.07	0.51	0.02	100.75	67	57	3	16	24	<6	21	27	13	<2	285	0.13
ER46	91.02	1.00	8.56	0.25	<0.01	0.08	0.32	<0.01	0.28	0.16	101.75	48	77	<2	22	28	<6	13	291	13	<2	337	0.19
ER47	90.05	0.72	8.15	0.12	0.02	0.10	0.18	0.10	0.77	<0.01	100.30	57	82	<2	17	20	<6	32	23	12	307	309	0.26
ER48	89.67	0.97	8.84	0.20	<0.01	0.08	0.14	0.16	0.67	0.02	100.85	44	71	<2	20	28	<6	33	48	14	476	343	0.20
ER49	90.16	1.08	8.47	0.32	<0.01	0.09	0.17	0.16	0.17	0.03	100.74	42	86	<2	23	27	<6	6	93	12	197	350	0.20
ER50	90.70	0.64	8.27	0.43	<0.01	0.14	0.22	0.80	0.24	0.02	101.51	50	74	<2	15	28	<6	12	30	13	31	280	0.10
ER51	89.72	1.17	8.92	0.32	<0.01	0.09	0.23	0.11	0.16	0.05	100.84	39	79	<2	24	53	<6	7	119	15	21	420	0.08
ER52	87.58	1.09	10.95	0.61	<0.01	0.08	0.18	0.28	0.15	0.02	101.00	63	85	<2	23	31	<6	5	62	15	6	352	0.08
ER53	90.29	1.23	7.47	0.53	<0.01	0.22	0.32	0.08	0.59	0.02	100.82	55	60	8	26	32	<6	20	26	13	9	354	0.11
ER54	90.34	1.23	7.43	0.52	<0.01	0.21	0.22	0.02	0.31	0.01	100.37	50	66	<2	26	64	<6	15	27	13	10	353	0.09
ER55	91.45	0.62	7.79	0.33	<0.01	0.16	0.14	0.19	0.33	<0.01	101.08	73	76	5	14	22	<6	18	21	12	17	305	0.13
ER56	90.07	0.77	8.97	0.41	<0.01	0.12	0.14	0.02	0.26	0.01	100.83	72	67	<2	18	20	<6	9	27	15	<2	314	0.12
ER57	88.34	0.94	9.89	0.58	<0.01	0.19	0.23	0.08	0.49	0.02	100.81	60	66	<2	20	28	<6	18	34	15	13	346	0.06
ER58	91.96	0.63	7.46	0.33	<0.01	0.13	0.17	0.03	0.58	0.01	101.36	68	68	<2	15	13	<6	14	24	14	3	300	0.12
ER59	88.53	1.38	9.60	0.69	<0.01	0.23	0.23	0.07	0.27	0.01	101.08	39	71	<2	29	47	8	16	28	15	9	393	0.19
ER60	91.78	0.52	7.36	0.40	<0.01	0.15	0.24	0.10	0.30	0.02	100.92	96	65	<2	12	24	<6	20	41	13	2	279	0.13
ER61	90.02	0.64	8.73	0.38	<0.01	0.08	0.30	0.29	0.20	0.01	100.71	39	71	3	14	21	<6	8	27	11	<2	255	0.14
ER62	89.74	0.66	9.36	0.41	<0.01	0.08	0.36	0.08	0.11	0.02	100.87	41	70	<2	15	24	<6	5	28	9	<2	246	0.19
ER65	91.88	0.56	7.16	0.57	<0.01	0.11	0.42	<0.01	0.12	0.02	100.87	42	58	<2	13	25	<6	6	18	10	<2	260	0.35
Hupper sand[a]																							
Mean	86.76	0.59	8.11	0.97	0.01	0.21	0.44	0.07	0.43	0.06		59.4	50.4	9.3	13.3	18.8	20.9	24.5	69.4	18.5	20.1	247.5	3.1
σ	7.66	0.31	5.82	1.52	0.01	0.24	0.87	0.19	0.69	0.09		100.2	36.5	17.8	5.8	15.5	23.3	38.7	93.0	4.3	27.4	102.1	1.8

[a] Chemical data for Hupper sand from Eramo [14].

Table 3
Normative calculation of the original mineral content of the two samples having the extremest compositions of Al_2O_3 and SiO_2

	Oxide	Wt.%	Mol.	Kln (mol)	Qtz (mol)	Kln (wt.%)	Qtz (wt.%)
ER43	SiO_2	92.04	1.53	0.14	1.39	16	84
	Al_2O_3	7.35	0.07	0.07	/		
ER41	SiO_2	86.93	1.47	0.22	1.25	25	75
	Al_2O_3	11.58	0.11	0.11	/		

Mineral abbreviations and formulae: quartz (Qtz, SiO_2); kaolinite (Kln, $Al_2O_3 \cdot 2SiO_2$).

on the stability relations between silica polymorphs after Fenner [15], is not reliable, because tridymite is not a stable phase in a pure silica system [8,21,22,46]. As tridymite forms only in the presence of some amount of alkali, its stability field is not only dependent on temperature and pressure, but also on chemical composition. In a pure silica system, the β-quartz ↔ β-cristobalite transition occurs above 1400 °C via an amorphous transition phase [46], and the crystalline order of cristobalite increases with temperature [42,47]. The variation of the structural order of cristobalite can be inferred by the $d_{(101)}$ values, which decrease as the formation temperatures increase [13,47]. For the crucible fragments from Derrière Sairoche, $d_{(101)}$ ranges from 0.4059 to 0.4068 nm ($\pm$0.0002). The $d_{(101)}$ data of cristobalite formed during the experimental runs at high temperature (1300−1700 °C) carried out by Eramo [13] on quartz−kaolinite briquettes were used as reference to estimate the temperature range recorded by the crucibles in the melting furnace. The $d_{(101)}$ values obtained in this study point to a temperature range between 1370 ($\pm$10) and 1500 °C ($\pm$50). Because of non-linear relation between cristobalite $d_{(101)}$ values and crystallization temperature, the uncertainty range of the inferred temperature varies according $d_{(101)}$ values [13].

Such a temperature range agrees well with that estimated (1330−1500 °C) by the same method [13] for the melting chamber of the furnace of Derrière Sairoche and with the highest liquidus temperature of the glass (1400 °C) produced in that glassworks [45].

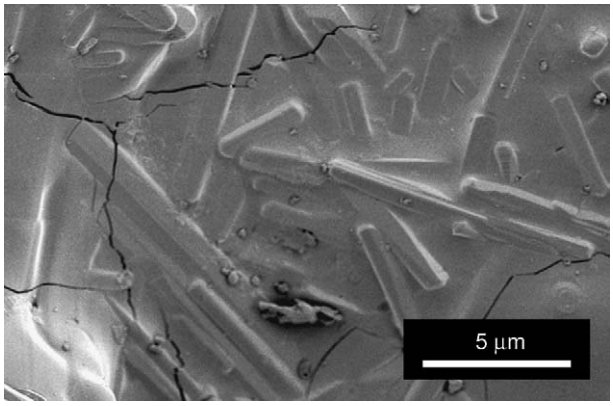

Fig. 7. Columnar microcrystals of mullite embedded in the silica-rich groundmass (ER30) (SEM, fresh fracture).

3.4. Two-steps firing

According to Biringuccio [41] and Diderot and D'Alembert [11], crucibles were fired in two steps: a preliminary firing in a fritting furnace and a final firing in the melting furnace before use. The restored crucibles (Chapter 2) show evident chromatic differences at the opposite parts of the long side, with colours ranging from purple to yellow through to grey. As the core of the crucible fragments shows the same chromatic heterogeneity observed in the restored crucibles, eight samples (yellow: ER22, 23, 34, 39; grey: ER21, 53, 57; purple: ER25) were analysed by UV−VIS spectrometry to investigate the influence of the oxidation state of iron on the colour of the ceramic body (Table 4). Iron reduction ratios (FeO/FeO_{tot}) [28] are clearly related to the three chromatic classes (Fig. 8). Since these colours are characteristic of specific portions of the crucible body, this should mean that they remained in the same position for a time long enough to change their iron-oxidation as a function of the local oxygen fugacity. Taking into account the crucible position in the melting chamber, the grey (or purple) side must have been exposed to the flame (reducing atmosphere), whereas the yellow side was next to the glory hole (oxidising atmosphere). As only fragments of the crucible wall were analysed, they represent the possible chromatic variability around the crucibles. This difference of iron-oxidation proves that the ceramic body was porous enough to allow some gas circulation when placed in the melting furnace. Thus, coloration of the crucible body occurred before surface vitrification, when differences in oxygen fugacity throughout the melting chamber could have affected the iron-oxidation state. Furthermore, the vitrification of the crucible body must have occurred in the melting furnace before its use, as shown by the sharp boundary between batch glass and the vitrified surface (Fig. 9). The surface certainly reached temperatures higher than those of the core of the crucible body since it received radiant energy either directly from the flame or reflected from the domed roof of the melting chamber. These thermal conditions favoured the *auto-glazing* of the surface at the expense of finer quartz and the amorphous phase formed after kaolinite decomposition. On the other hand, mullite is more resistant than quartz and its presence in the densified zone (Fig. 10a, b), between the vitrified layer and the crucible body, hinders the diffusion of alkalies into the latter [12].

Table 4
FeO and FeO_{tot} concentrations (wt.%) by UV−VIS spectrometry and XRF, with iron reduction ratios

Sample	Colour	FeO	FeO_{tot}	FeO/FeO_{tot}
ER21	grey	0.34	0.56	0.61
ER22	yellow	0.12	0.38	0.32
ER23	yellow	0.10	0.59	0.16
ER25	violet	0.29	0.32	0.89
ER34	yellow	0.10	0.45	0.23
ER39	yellow	0.10	0.46	0.22
ER53	grey	0.25	0.48	0.51
ER57	grey	0.31	0.53	0.57

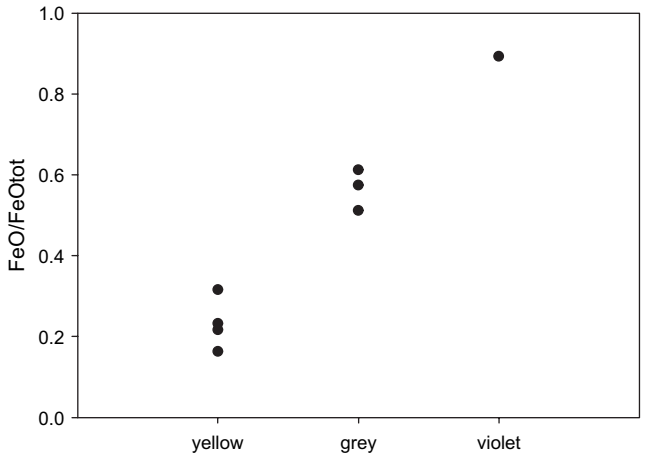

Fig. 8. Body colours vs. the oxidation state of iron. The iron reduction ratio increases from yellow to purple, i.e. toward more reducing conditions [28].

Taking into account that the metastable melting point of β-quartz falls between 1400 and 1450 °C [27,37] and that above 1500 °C the rate of fusion of quartz exceeds the rate of crystallization of amorphous silica to form cristobalite [42], it is reasonable that the vitrified layer started to form at temperatures above 1450 °C. However, an incipient vitrification at lower temperatures due to the reaction of KOH dispersed in the furnace gases with the silica phases present on the crucible surface cannot be excluded (see below).

To place the dried crucibles in the melting furnace during its activity would have broken these pots due to the large thermal gradient. Consequently, a preliminary low sintering (800–1000 °C) in the oven annexed to the melting furnace [19] must have taken place.

Although one knows from historical sources that crucibles withstood for some months on average [31,34,35], the occurrence of metastable quartz shows that the kinetics of the polymorphic transformations were very slow, despite of the kinetics of the kaolinite dehydroxilation.

In conclusion, both the oxidation state of iron and the surface vitrification occurred before the use of the crucibles, this supports the technological information coming from the old treatises about the firing in two steps.

3.5. Chemical contaminations

Under service conditions, crucibles interact with batch glass and gases, which affect their properties. In the literature, the chemical attack by fluids is known as corrosion [10,26,38]. Generally speaking, the furnace gases corrode the exterior of the pots, while the glass corrodes the interior. The basic process of corrosion is diffusion controlled. The rate of diffusion at the refractory surface rules the rate of the process [48]. The driving force of the corrosion due to glass is the difference in the concentrations of the refractory components in the glass and at the refractory/glass interface [9]. For a given composition, the corrosion rate is inversely proportional to glass viscosity and then directly proportional to temperature [48]. Davis [10] reports that a temperature increase of 50 °C upon the melting point of a given glass will double the corrosion rate.

The crucible surface, as well as the furnace roof, is exposed to the corrosive attack of the furnace gases. Alkali volatilisation is one of the main actors in the refractory corrosion and its rate depends on the type of fuel (i.e. wood, oil, methane, etc.), on the water vapour concentration and on the furnace gas velocity [49]. In wood-fed furnaces alkali volatilisation occurring during combustion, makes a relevant contribution to that coming from the batch during the melting process. The corrosion mechanism due to alkali-bearing species present in the furnace gas can be synthesized in the following chemical reactions [1]:

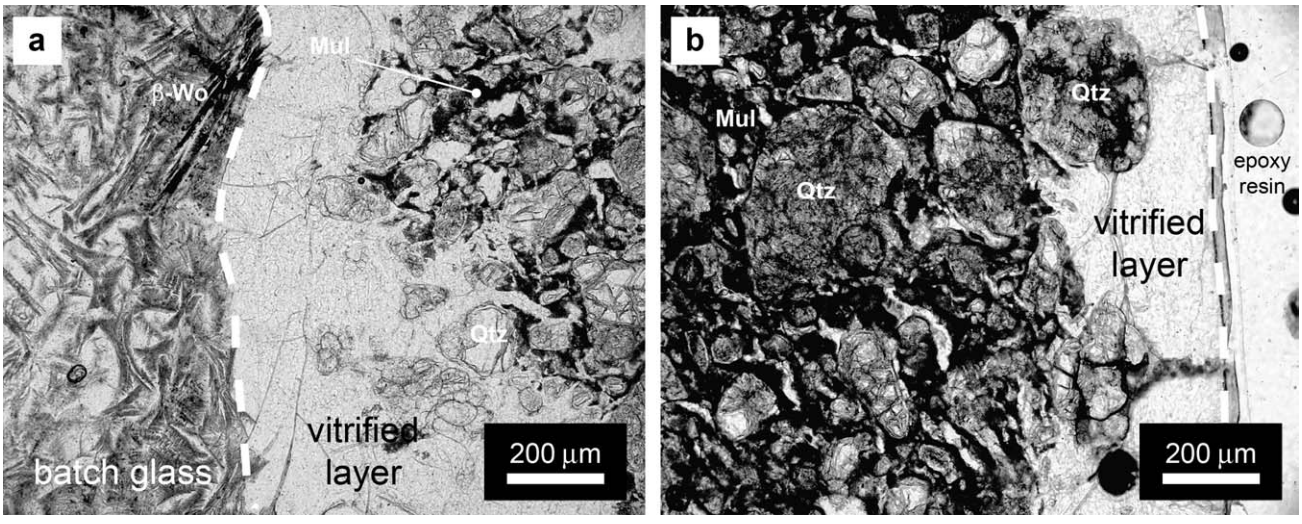

Fig. 9. The opposite surfaces of ER38 observed in plane light under the optical microscope. (a) The batch glass adhering to the vitrified layer shows a quench texture (β-wollastonite crystals) and gives evidence of its chemical and physical difference from the vitrified layer of the crucible. (b) The crystalline core shows a relevant amount of quartz with seriate texture surrounded by a densified microcrystalline matrix, which turns into a vitrified layer outward. Mul = mullite, Qtz = quartz, β-Wo = β-wollastonite.

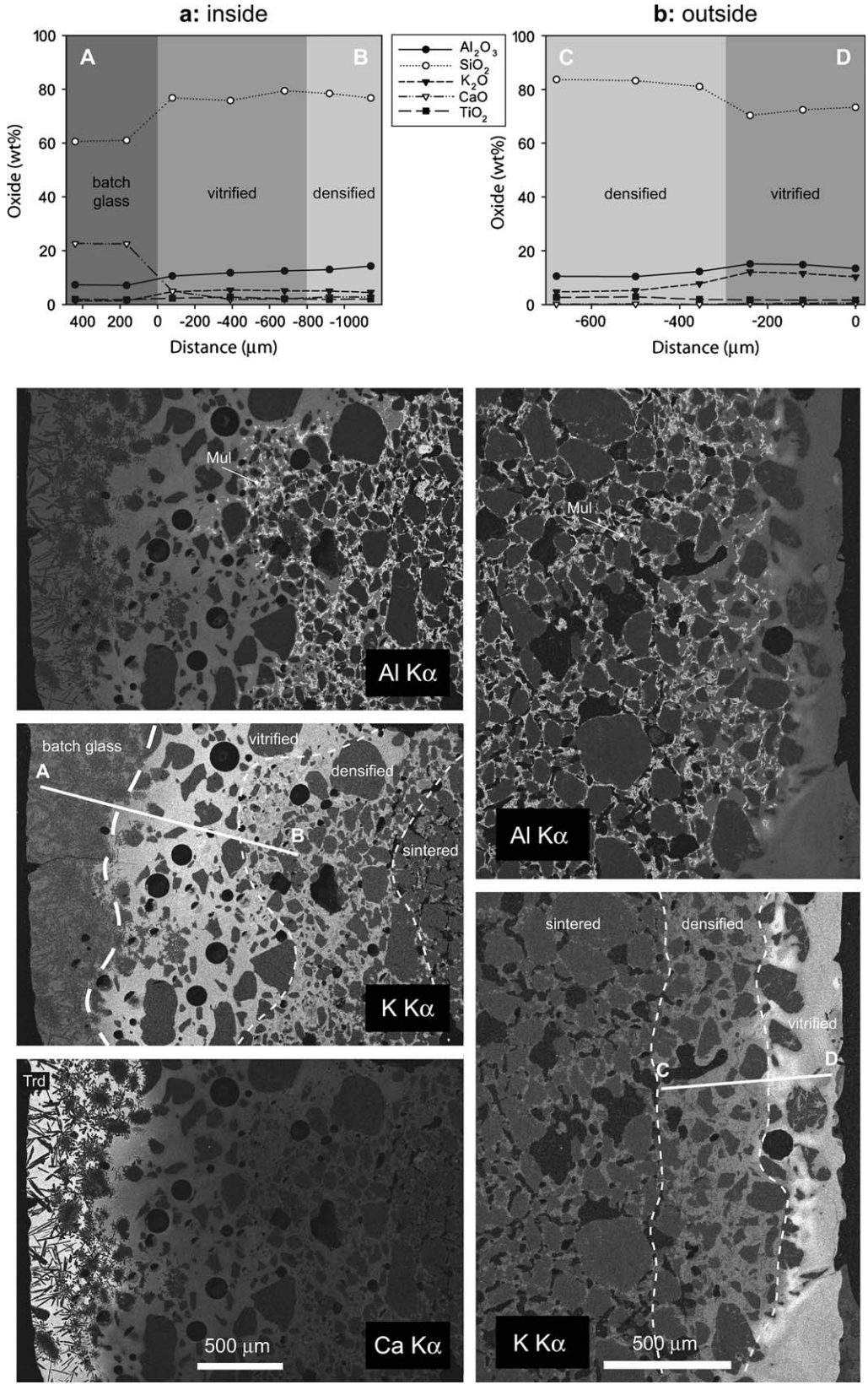

Fig. 10. Change in chemical composition (EDS) and X-ray maps of selected elements (Al, K and Ca) of the surface in contact with batch glass (a) and the outer surface (b) in ER42. (a) The corrosion zone (vitrified and densified layers) is characterized by potassium enrichment and very limited diffusion of Ca from batch glass. Acicular and columnar tridymite occurs in the batch glass adhering to the crucible in a Ca-rich glassy matrix. Vesiculation (black areas) is present in the vitrified sub-zone, while porosity decreases in the densified sub-zone. The crystalline core shows porosity developed during sintering. The boundary between the vitrified and densified areas (central dashed line in the K-map) is marked by the presence/absence of mullite aggregates (brightest zones in Al-map). (b) The outer surface shows similar fabric variation as observed in the inner surface. The vitrified layer shows coarse relic quartz in a glassy matrix enriched with potassium. The densified zone contains mullite aggregates not yet dissolved by the glassy matrix. Mul = mullite, Qtz = quartz, Trd = tridymite.

Table 5
Chemical profile by EDS through the batch glass/crucible interface (Fig. 10a)

Distance[a] (μm)	Na_2O (wt.%)	MgO (wt.%)	Al_2O_3 (wt.%)	SiO_2 (wt.%)	P_2O_5 (wt.%)	K_2O (wt.%)	CaO (wt.%)	TiO_2 (wt.%)	MnO (wt.%)	Fe_2O_{3tot} (wt.%)	Total (wt.%)
440	0.4	2.5	7.3	60.6	2.5	1.4	22.6	1.9	0.3	2.1	101.4
165	0.4	2.3	7.1	61.0	2.5	1.4	22.5	1.8	0.7	2.1	101.7
−80	0.6	0.1	10.6	76.8	0.0	4.7	4.9	2.3	0.0	0.2	100.2
−390	0.5	0.0	11.7	78.8	0.1	5.4	1.9	2.4	0.0	0.3	101.1
−680	0.5	0.5	12.4	79.4	0.4	5.1	2.0	1.9	0.0	0.5	102.8
−920	0.4	0.7	13.0	78.4	0.1	5.0	1.8	1.9	0.0	0.4	101.6
−1140	0.5	0.8	14.2	76.7	0.4	4.5	1.7	2.0	0.0	0.5	101.3

[a] The batch glass/crucible interface was taken as origin. Positive values are toward the batch glass and negative values are toward the core of the crucible body.

$$M_2O\ (\text{batch and wood}) + H_2O\ (\text{combustion gas}) \leftrightarrow 2MOH\ (\text{gas}) \quad (1)$$

$$2MOH\ (\text{gas}) \leftrightarrow M_2O\ (\text{dissolved in the silica}-\text{rich liquid layer}) + H_2O\ (\text{combustion gas}) \quad (2)$$

where M = K or Na.

The alkali-bearing phases present in the batch as well as in the wood fuel react with the combustion-generated water vapour to form alkali hydroxides (1). The interaction of these hydroxides with the silica-rich liquid surface of the crucibles, dissolves M_2O in it and gives back water vapour (2). According to observations by Allendorf and Spear [1], higher refractory temperatures decrease the alkali concentration in the silica-rich liquid layer and inhibit corrosion.

In the Derrière Sairoche samples, both surfaces show partial melting. The surface not in contact with glass shows a vitrified layer with a quite homogeneous thickness (auto-glazing). On the contrary, the vitrified layer of the surface in contact with the batch glass is more extended and irregular due to corrosion. The occurrence of β-wollastonite or tridymite as first phase crystallized from the batch glass is due to the CaO/SiO_2 ratio (Figs. 9a, 10a). It is worth noting that neither β-wollastonite nor tridymite crystallized in the vitrified layer.

X-ray maps give evidence of an enrichment of K in the vitrified layers (inner and outer surfaces) compared to the core of the crucible body and a limited calcium diffusion in the vitrified layer next to the batch glass as well (Fig. 10a). Both in the inner and outer surfaces, mullite aggregates mark the boundary between the crystalline body and vitrified layer of the crucibles. Differences in geometry and in chemical composition (Tables 5 and 6) between the two vitrified layers, point to two distinct sources of contamination.

The batch glass/crucible interface is characterized by chemical diffusion between two liquids (i.e. batch glass and vitrified layer) with different viscosity. Their different degree of polymerization, related to the SiO_2 concentration, is responsible for the chemical partitioning of such oxides as K_2O, CaO, MgO and P_2O_5 [39,50]. Fig. 10a shows the lateral chemical variation of the batch glass/crucible interface, where, despite K_2O migrating to the vitrified layer, CaO essentially remained in the batch glass. The chemical trends through the interface glass/crucible for medieval crucibles reported by Merchant et al. [29] point to similar diffusion patterns. Although the batch glass is the source of K_2O present in the vitrified layer, some contribution from the furnace gases cannot be excluded. The diffusion of K_2O from the batch glass into the vitrified layer of the crucible represents the principal agent of corrosion, because it lowers the viscosity of the vitrified silica-rich layer and the melting temperature of the crucible body.

The outer surface (Fig. 10b), not in contact with batch glass, revealed a quite homogeneous potassium distribution in the vitrified layer (~300 μm). Because of mullite dissolution, Al_2O_3 concentration in the vitrified layer is higher than in the densified layer. Only coarser quartz grains withstood dissolution. The very low content of calcium in the glassy matrix of the outer surfaces excludes batch glass as a possible origin of potassium contamination and points to the furnace gases (Fig. 10b). When wood fuel is used, combustion temperatures above 900 °C causes the volatilisation of elements such as potassium, Na, S, B and Cu if originally present in the wood [32]. Chemical analyses of ash samples obtained by wood from the valley of Chaluet [45] show that only

Table 6
Chemical profile by EDS through the crucible surface not in contact with batch glass (Fig. 10b)

Distance[a] (μm)	Na_2O (wt.%)	MgO (wt.%)	Al_2O_3 (wt.%)	SiO_2 (wt.%)	P_2O_5 (wt.%)	K_2O (wt.%)	CaO (wt.%)	TiO_2 (wt.%)	MnO (wt.%)	Fe_2O_{3tot} (wt.%)	Total (wt.%)
−680	0.1	0.2	10.5	83.7	0.1	4.7	0.1	1.6	0.0	0.8	101.9
−500	0.0	0.1	10.4	83.3	0.0	5.2	0.2	1.9	0.1	0.9	102.0
−355	0.1	0.1	12.3	80.1	0.1	7.8	0.2	0.9	0.0	0.8	102.3
−240	0.0	0.0	15.1	70.8	0.0	12.1	0.1	0.7	0.0	0.7	99.6
−120	0.1	0.1	14.8	72.4	0.2	11.6	0.4	0.6	0.0	0.9	101.1
0	0.0	0.2	13.4	73.4	0.2	10.3	0.3	0.7	0.1	1.0	99.5

[a] Negative values are from the surface toward the core of the crucible body.

potassium occurs in relevant concentration. Further, K_2O present in the batch glass is also subject to volatilisation during the melting process and together with K_2O coming from wood combustion will be dispersed in the furnace gases and diffused through the hot and viscous surface of the crucibles. This process is also advocated for the vitrified surface of the refractory lining of the melting furnace of Derrière Sairoche [13].

EDS analyses showed that in the vitrified layer of the outer surface K_2O ranges from 5 to 12 wt.% and in the vitrified layer of the inner surface from 4 to 5 wt.%. Since K_2O is the principal contaminant in both inner and outer crucible surfaces, the ternary system $K_2O-SiO_2-Al_2O_3$ (KSA) [33] may be appropriate to explain the corrosion mechanism, even though the rest of the oxides were not considered for the sake of simplicity. Fig. 11 shows part of the KSA system with the isothermal cuts at 1370 and 1500 °C, which are the lower and the upper temperatures determined in this study for the analysed crucible bodies. The isothermal cuts depict the compatibility fields of liquid (L) and solid phases (Mul, Trd/Crs and Lct) in the portion of interest of the ternary diagram KSA. On the $SiO_2-Al_2O_3$ side, a segment which shows the approximated compositional range of the crucible body and two lines to join the K_2O corner (not shown) were drawn. This area represents the theoretical compositional field of the corrosion products after K_2O attack. As shown in the same diagram, the compositional points of the actual corrosion products are instead shifted toward the Al_2O_3 corner, because of non-complete dissolution of quartz and mullite (Fig. 11).

By varying the concentration of K_2O in the corrosion product, the compatibility field at a given temperature will change. For low concentrations of K_2O, mullite, silica and a liquid L_1 will coexist in equilibrium. Higher amounts of potassium will move the composition of the corrosion product in the compatibility field where mullite and liquid are in equilibrium. By further increase of K_2O, the composition will fall inside the liquid field. Where the compositional field of the corrosion products overlaps the compatibility fields of the isothermal cut at 1500 °C, it can be seen that, when K_2O is above 4 wt.%, all is liquid. On the other hand, at 1370 °C concentrations above 7 wt.% of K_2O are necessary to obtain a complete liquid phase.

Inner and outer surfaces all have potassium in the glassy matrix. The highest concentrations of K_2O are reached in the vitrified layer in both cases. According to Fig. 11, the compositional points should have been in the liquid field, or at least on the boundary curve between the liquid field and the compatibility field where mullite and liquid coexist. The compositional points of the vitrified zone of the outer surface, belong to the former case, while those of the inner surface belong to the latter. The compositional points of the densified layers are close to the boundary curves at 1370 and 1500 °C between the liquid field and the compatibility field of mullite and liquid. This explains the coexistence of mullite and glassy matrix. The presence of a glassy matrix increases the diffusion rate of potassium toward the core of the crucible body. The proximity of the compositional points of both surfaces to the boundary curves at 1370 and 1500 °C between the

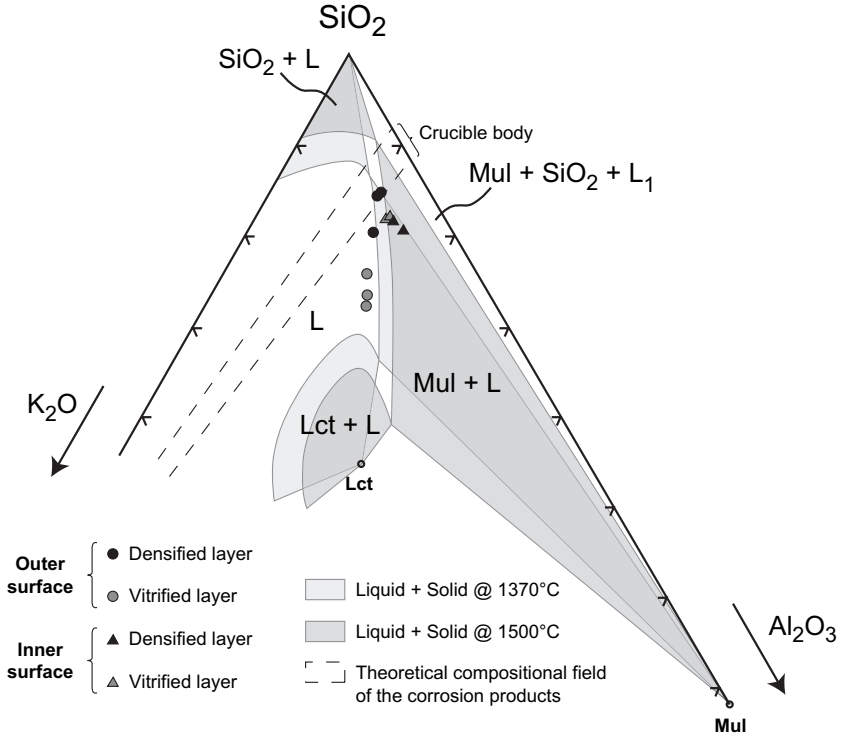

Fig. 11. Area of interest of the $K_2O-SiO_2-Al_2O_3$ system, showing the stability fields of the isothermal cuts at 1370 and 1500 °C. The compositional points of the glassy matrix of the inner and outer crucible surfaces fall in proximity of the boundary curve between the liquid field (L) and the compatibility field of mullite and liquid (Mul + L_1). Mul = mullite, Lct = leucite, SiO_2 = tridymite and/or cristobalite, L = liquid, L_1 = liquid in equilibrium with mullite.

liquid field and the compatibility field of mullite and liquid, supports the temperature range estimated for the crucibles and validates a posteriori the approximations made to the chemical compositions of the glassy matrix plotted in the KSA system.

To summarize, the K_2O attack on crucibles acts on both the surface in contact with batch glass and the surface which is not. In the former, the preferred diffusion of alkali metals from batch glass to the crucible body is the main cause of corrosion, as can be further observed in the reaction zone between soda-lime glass and alumina-silica refractories in the modern glass industry [12]. In the latter, the alkali hydroxide gases dispersed in the furnace gases corrode the crucible surface by dissolution of alkali oxides in the silica-rich liquid layer. Owing to the use of wood as fuel, their concentration is supposed to be higher than that present in modern tank furnaces.

4. Summary

By analysing the crystalline core of the crucible, an original mineral composition of quartz sand (~80 wt. %) and kaolinite (~20 wt.%) was determined. The homogeneous chemical composition points to a single source of raw materials. Furthermore, petrographical and chemical features allow to exclude recycling of crucible fragments as temper. These interpretations are in agreement with findings by Eramo [14], who reported a good correspondence between the crucibles and some of the local refractory earth (Hupper sand) samples.

The crucibles were fired and used in a temperature range between 1370 and 1500 °C.

The different oxidation states of iron in the crucible fragments prove that they were placed in the melting furnace before the densification of the ceramic body occurred. It can be inferred that the iron-oxidation changed as a function of the oxidising (next to glory hole) or reducing (next to the flame) atmosphere. The sharp boundary between glass and vitrified surface shows that the vitrification of the crucible body occurred before use, supporting the thesis that crucibles received (at least) the last firing in the melting furnace at temperatures as high as 1500 °C.

The corrosion of the crucible by alkali attack was observed on both, the surface in contact with batch glass and the surface not in contact with batch glass.

In the first case, the chemical diffusion of potassium from the molten glass and, in the second case, potassium dissolution from the furnace gases to the silica-rich vitrified layer of the crucible, reduced its melting temperature and weakened the structure.

Acknowledgments

This paper is part of a Ph.D. thesis under the direction of Prof. M. Maggetti and of Dr. G. Thierrin-Michael (University of Fribourg). The author is grateful to them for their invaluable guidance in my research and constructive criticism in the preparation of this paper. Dr. V. Serneels for X-ray fluorescence analyses and his enlightening remarks. Thanks are also due to Mr. C. Neururer for his assistance on EDS analyses. Prof. B. Grobéty (University of Fribourg) is kindly acknowledged for his suggestions. The author is indebted to Mr. C. Gerber and Mr. N. Stork of the Archaeological Survey of Canton Bern for their kind collaboration. Two anonymous referees are specially thanked for their careful reviews.

Appendix 1. Analytical methods

Sample preparation: In order to avoid contamination, the vitrified surfaces of the samples were mechanically removed. Between 5 and 10 g of the crystalline core was powdered by means of a tungsten carbide (WC) ball-mill.

Optical microscopy (OM): Petrographic analyses were carried out on thin sections under a polarising microscope Carl Zeiss ''Standard RP 48-66/6''.

X-ray fluorescence (XRF): Bulk chemical analyses were performed on glass tablets using a PHILIPS PW 2400 X-ray fluorescence spectrometer equipped with a rhodium X-ray tube. The glass tablets were obtained by melting together in a Pt crucible ($T = 1150$ °C; $t = 10$ min) 0.700 g of calcined sample's powder with 0.350 g of LiF and 6.650 g of $B_4Li_2O_7$ using a PHILIPS PERL'X-2 machine.

UV−VIS spectrometry: Fifty grams of each sample was dissolved in an acid solution (HF:H_2SO_4, 1:1) and mixed with a buffer solution which gave a red complex in presence of iron. FeO concentration was determined by multiplying the absorbency value ($\lambda = 528$ nm), obtained by a UVIKON XS spectrometer, for the regression coefficient calculated after the calibration procedure. A detailed description of the sample and the standard preparation is provided by Fries and Getrost [16].

X-ray diffraction (XRD): X-ray diffraction analyses were carried out on a PHILIPS PW1800 diffractometer with Cu K_α radiation at 40 kV and 40 mA (step angle of 0.02°, 2θ from 2° to 65°, measuring time 1 s per step).

Loss on ignition (LOI): Loss on ignition was determined by heating 2 g of sample at 1000 °C for 1 h.

Scanning electron microscopy (SEM): Secondary electron (SE) and back-scattered images (BSE) were taken by an FEI SIRION XL 30S FEG scanning electron microscope (operating in a range of 5−20 kV). Qualitative and quantitative chemical compositions were obtained by energy dispersive spectrometry (EDS) using an EDAX NEW-XL30 detector. X-ray maps of Si, Al, K and Ca were performed (accelerating potential = 15 kV, counting time = 11 h) on the surfaces of the crucible fragments to examine the chemical contamination. Quantitative EDS measure was obtained using Corning glass D [6] as standard. The operating conditions were accelerating potential = 15 kV, beam current = 1.2 nA, spot size = 6 × 4 μm, measuring time = 50 s. The precision and accuracy were determined after five measurements on the same analysis point of the Corning glass standard D (Table 7). The former is expressed as relative standard deviation (standard deviation × 100%/mean)

Table 7
Precision and accuracy of measured major and minor oxides of the Corning glass standard D [6]

Oxide	Reference (wt.%)	Measure 1 (wt.%)	Measure 2 (wt.%)	Measure 3 (wt.%)	Measure 4 (wt.%)	Measure 5 (wt.%)	Mean (wt.%)	σ (wt.%)	σ_{rel} (%)	e_{rel} (%)
Na_2O	1.2	0.9	0.9	1.0	0.9	1.1	1.0	0.1	8.9	18.3
MgO	3.9	4.0	4.1	3.8	3.9	4.0	4.0	0.1	2.2	0.3
Al_2O_3	5.3	5.4	5.5	5.3	5.3	5.4	5.4	0.1	1.6	0.9
SiO_2	57.2	56.9	57.6	57.3	57.2	57.3	57.3	0.3	0.5	0.1
P_2O_5	3.9	3.9	3.9	4.0	3.9	3.7	3.9	0.1	3.1	1.4
K_2O	11.3	11.3	11.2	11.2	11.3	11.2	11.2	0.1	0.6	0.6
CaO	14.8	14.6	14.8	14.7	14.7	14.8	14.7	0.1	0.5	0.5
TiO_2	0.4	0.4	0.4	0.4	0.3	0.2	0.3	0.1	17.1	12.1
MnO	0.6	1.2	0.9	0.7	0.9	0.7	0.8	0.2	24.4	53.8
Fe_2O_{3tot}	0.5	1.0	1.3	0.8	0.4	0.8	0.8	0.3	37.7	63.1

and the latter as relative error ((|observed composition − reference composition|/certified composition)100%).

References

[1] M.D. Allendorf, K.E. Spear, Thermodynamic analysis of silica refractory corrosion in glass-melting furnaces, Journal of the Electrochemical Society 148 (2) (2001) B59−B67.

[2] G. Amweg, in: Les Arts dans le Jura bernois et à Bienne, Tome II, Arts appliqués, Porrentruy, 1941.

[3] J.R. Ashworth, Transformation mechanisms of tridymite to cristobalite studied by transmission electron microscopy, Physics and Chemistry of Minerals 15 (1988) 246−251.

[4] M. Bellotto, A. Gualtieri, G. Artioli, S.M. Clark, Kinetic study of the kaolinite−mullite reaction sequence. Part I: kaolinite dehydroxylation, Physics and Chemistry of Minerals 22 (1995) 207−214.

[5] M. Bellotto, A. Gualtieri, G. Artioli, S.M. Clark, Kinetic study of the kaolinite−mullite reaction sequence. Part II: mullite formation, Physics and Chemistry of Minerals 22 (1995) 215−222.

[6] R.H. Brill, Tables of analyses, in: Chemical Analysis of Early Glasses, vol. 2, The Corning Museum of Glass, New York, 1999.

[7] V. Brumm, Un pays du verre et du cristal les Vosges du nord au siecle des lumieres, Mémoire de maîtrise d'histoire réalisé par Véronique Brumm, Université des sciences humaines de Strasbourg, Strasbourg, 1997.

[8] M.J. Buerger, The stuffed derivative of the silica structures, American Mineralogist 39 (1954) 600−614.

[9] A.R. Cooper Jr., Dissolution kinetics in glass making, in: Advances in Glass Technology, Technical Papers of the VI International Congress on Glass, Washington, D.C. USA, July 8−14, 1962, compiled by the American Ceramic Society, Columbus, Ohio, 1962, pp. 217−229.

[10] A.D. Davis, Refractories for glass melting, in: M.B. Bevers (Ed.), Encyclopedia of Materials Science and Engineering, Pergamon, Oxford, 1986, pp. 4134−4140.

[11] D. Diderot, J. D'Alembert, L'art du verre, reprint 2002, in: Encyclopédie ou dictionnaire raisonné des sciences, des arts et des métiers, vol. 17, Inter-Livres, 1771.

[12] W. Eitel, Ceramics and hydraulic binders, in: Silicate Science, vol. V, Academic Press, New York, 1966.

[13] G. Eramo, The melting furnace of the Derrière Sairoche glassworks (Court, Swiss Jura): heat-induced mineralogical transformations and their technological signification, Archaeometry 47 (3) (2005) 571−592.

[14] G. Eramo, Pre-industrial glassmaking in Swiss Jura: the refractory earth for the glassworks of Derrière Sairoche (Ct. Bern, 1699−1714), in: M. Maggetti, B. Messiga (Eds.), Geomaterials in Cultural Heritage, Archaeometric Special Publication, Geological Society of London, in press.

[15] C.N. Fenner, The stability relations of the silica minerals, American Journal of Science 36 (1913) 331−384.

[16] E. Fries, H. Getrost, Organische Reagenzien für die Spurenanalyse, Merck, Darmstadt, 1975.

[17] C. Gerber, Fouille d'une verrerie forestière du début du XVIIIe siècle à Court (Jura suisse), Bulletin de l'Association pour l'Archéologie du verre (2000) 14−15.

[18] C. Gerber, Court-Chaluet − A la découverte d'une verrerie jurassienne du 18e siècle, Bern, Nike Bulletin 1 (03) (2003) 14−18.

[19] C. Gerber, Court-Chaluet bei Moutier (Berner Jura, Schweiz): eine Schwarzwälder Glasshütte, in: P. Steppuhn (Ed.), Glashütten im Gespräch. Berichte und Materialien vom 2 Internationalen Symposium zur archäologischen Erforschung mittelalterlicher und frühneuzeitlicher Glashütten Europas, Verlag Schmidt-Römhild, Lübeck, 2003, pp. 64−69.

[20] J. Hétru, Le verre: l'art et la matière, Editions Bertout, Luneray, 1996.

[21] V.G. Hill, R. Roy, Silica structure studies, VI, on tridymite, Transactions of the British Ceramic Society 57 (1958) 496−510.

[22] S.B. Holmquist, Conversion of quartz to tridymite, Journal of the American Ceramic Society 44 (1961) 82−86.

[23] J.G. Hawthorne, C.S. Smith, Theophilus, On Divers Arts, Book 2: The Art of the Worker in Glass, Dover Publications, New York, 1979.

[24] C.M. Jackson, L. Joyner, C.A. Booth, P.M. Day, E.C.W. Wager, V. Kilikoglou, Roman glass-making at Coppergate, York? Analytical evidence for the nature of production, Archaeometry 45 (2003) 435−456.

[25] S. Lee, Y.J. Kim, H. Moon, Phase transformation sequence from kaolinite to mullite investigated by energy-filtering transmission electron microscope, Journal of the American Ceramic Society 43 (1999) 2841−2848.

[26] W.E. Lee, W.M. Rainforth, Ceramic Microstructure. Property Control by Processing, Chapman & Hall, London, 1995.

[27] J.D. Mackenzie, Fusion of quartz and cristobalite, Journal of the American Ceramic Society 43 (1960) 615−620.

[28] M. Maggetti, G. Galetti, R. Schneuwly, Die Feinkeramik von Sissach-Brühl: eine spätlatènezeitliche Referenzgruppe, Archäologie und Museum, Amt für Museen und Archäologie des Kantons Baselland, 1988 pp. 2−46.

[29] I. Merchant, J. Henderson, D. Crossley, M. Cable, Medieval glass-making technology: the corrosive nature of glass, in: A. Sinclair, E. Slater, J. Gowlett (Eds.), Archaeological Sciences, Liverpool, 1995, Oxbow Monograph 64, 1997.

[30] C. Merret, The art of glass, original version: L'Arte vetraria by Antonio Neri, London, 1662.

[31] G.J. Michel, Verriers et verreries en Franche-Comté au XVIIIème siècle (2 tomes), Editions ERTI, 1989.

[32] M.K. Misra, K.W. Ragland, A. Baker, Wood ash composition as a function of furnace temperature, Biomass and Bioenergy 4 (2) (1993) 103−116.

[33] E.F. Osborn, A. Muan, Phase Equilibrium Diagrams of Oxide Systems, Plate 5, The American Ceramic Society and the Edward Orton, Jr., Ceramic Foundation, 1960.

[34] P. Piganiol, Le verre. Son histoire. Sa technique, Hachette, Paris, 1965.

[35] C. Pris, La manufacture royale des glaces de Saint-Gobain, Une grande entreprise sous l'Ancien Regime. Part II − Travail, Paris, 1975, pp. 371−705.

[36] T. Rehren, Rationales in old world base glass compositions, Journal of Archaeological Science 27 (2000) 1225−1234.

[37] P. Richet, Y. Bottinga, L. Deneilou, J.P. Petitet, C. Tequi, Thermodynamic properties of quartz, cristobalite and amorphous SiO_2: drop calorimetry measurements between 1000 and 1800 K and a review from 0 to 2000 K, Geochimica et Cosmochimica Acta 46 (1982) 2639−2658.

[38] A.B. Searle, Refractory Materials: Their Manufacture and Use, Charles Griffin & Co. Ltd., London, 1953.

[39] C.S.J. Shaw, The effect of experiment geometry on the mechanism and the rate of dissolution of quartz in basanite at 0.5 GPa and 1350 °C, Contribution to Mineralogy and Petrology 139 (2000) 509−525.

[40] A. Shugar, T. Rehren, Formation and composition of glass as a function of firing temperature, Glass Technology 43 (C) (2002) 145−150.

[41] C.S. Smith, M.T. Gnudi, The Pirotechnia of Vannoccio Biringuccio, M.I.T. Press, Massachussets, 1966.

[42] R.B. Sosman, The Phases of Silica, Rutgers University Press, New Brunswick, New Jersey, 1965.

[43] K. Srikrishna, G. Thomas, R. Martinez, M.P. Corral, S. De Aza, J.S. Moya, Kaolinite−mullite reaction series: a TEM study, Journal of Material Science 25 (1990) 607−612.

[44] W.B. Stern, Zur chemischen Analyse der Bieler Gläser, in: R. Glatz (Ed.), Hohlglasfunde der Region Biel, Zur Glasproduktion im Jura, HAUPT, Bern, 1991, pp. 83−86.

[45] W.B. Stern, Y. Gerber, Potassium−calcium glass: new data and experiments, Archaeometry 46 (2004) 137−156.

[46] S.J. Stevens, R.J. Hand, J.H. Sharp, Polymorphism of silica, Journal of Material Science 32 (1997) 2929−2935.

[47] A.G. Verduch, Kinetics of cristobalite formation from silicic acid, Journal of the American Ceramic Society 41 (1958) 427−432.

[48] F.E. Woolley, Prediction of refractory corrosion rate from glass viscosity and composition, in: L.J. Trostel Jr. (Ed.), UNITECR '89 Proceedings, The American Ceramic Society, Ohio, 1989, pp. 768−779.

[49] K.T. Wu, H. Kobayashi, Three-dimensional modelling of alkali volatilisation/crown corrosion in oxy-fired glass furnaces, in: G.A. Pecoraro, J.C. Marra, J.T. Wenzel (Eds.), Corrosion of Materials by Molten Glass, Ceramic Transactions, vol. 78, The American Ceramic Society, Ohio, 1996, pp. 205−216.

[50] Y. Zhang, D. Walker, C.E. Lesher, Diffusive crystal dissolution, Contributions to Mineralogy and Petrology 102 (1989) 492−513.